REACTIVATION OF SEA-URCHIN SPERM FLAGELLA INDUCED BY RAPID PHOTOLYSIS OF CAGED ATP

TOMOMI TANI* AND SHINJI KAMIMURA

Department of Biology, Graduate College of Arts and Sciences, University of Tokyo, Komaba, Meguro-ku 3-8-1, Tokyo 153, Japan

*e-mail: tani@nano.c.u-tokyo.ac.jp

Summary

Sea-urchin sperm flagella in a state of rigor were reactivated by rapid photolysis of caged ATP. After a time lag of 11–17 ms, all bends in the axonemes present during rigor began to be propagated towards the tip as if their propagation had not been interrupted. This result suggests that the site-specific activity of dyneins along the length of the axoneme is preserved even during rigor states when ATP is absent and that regulation of the activity can be restarted immediately with a new cycle of ATP turnover. During the starting transient, pre-existing rigor waves in the distal region were propagated without a change in the maximal shear angle until they disappeared at the tip. This was more evident when the rapid reactivation was triggered in high-viscosity solution, in which only the form of new bends was greatly affected by viscous load. After reactivation, the velocity of microtubule sliding increased and reached a plateau within 28 ms. This time course reflects the rate of force generation by dynein *in situ*.

Key words: sea-urchin, spermatozoon, flagellum, motility, dynein, caged ATP, axoneme, bend initiation, bend propagation, microtubule sliding, presteady-state kinetics, viscous load, *Anthocidaris crassispina*.

Introduction

Bending in eukaryotic flagella results from active sliding between axonemal microtubules caused by the force exerted during ATP hydrolysis by dynein (Gibbons and Rowe, 1965; Satir, 1968; Summers and Gibbons, 1971; Shingyoji *et al.* 1977; Brokaw, 1989). However, the mechanism regulating bend initiation and propagation is not clearly understood. In flagella with planar bends, regular alternation of active sliding is thought to occur between the two halves of the axoneme accompanied by a passive retrograde sliding on the opposite side of the axoneme, since active sliding by dynein arms occurs in one direction only (Sale and Satir, 1977).

To investigate chemo-mechanical coupling during flagellar motility, it is necessary to understand how the local activity of ATPase and the sliding of microtubules are regulated in the axoneme. Studies have established that the relationship between the beat frequency of reactivated flagella and ATP concentration shows a good fit to the Michaelis–Menten equation and that an estimated average of 1–2 ATP molecules are hydrolyzed per dynein arm during a single beat cycle (Brokaw and Benedict, 1968; Gibbons and Gibbons, 1972). However, the exact region of active sliding within beating flagella has yet to be identified, and it is not clear which intermediate state during ATPase activity is involved in force generation by dynein.

To examine these problems more closely, tritonated axonemes with rigor waves (Gibbons and Gibbons, 1974*a*) were reactivated by rapid photolysis of caged ATP, and the subsequent changes in the waveforms were analyzed in detail. Such experiments are expected to provide insight into the chemo-mechanical coupling of dynein arms, since all dynein arms in ATP-depleted medium are thought to be in a state of rigor (Gibbons and Gibbons, 1974*b*) and capable of reactivation in a synchronized manner.

Several investigators have described such experiments, for example, by the rapid local application of ATP to axonemes in rigor using an iontophoretic technique (Shingyoji *et al.* 1977) or by homogeneous application of ATP by perfusion (Goldstein, 1979). In the present study, a synchronous and homogeneous application of ATP to the whole length of an axoneme in rigor was achieved using the technique of rapid photolysis of caged ATP (Kaplan *et al.* 1978; McCray *et al.* 1980; Goldman *et al.* 1982; Woolley and Bozkurt, 1995). Once reactivated, the starting transient of angular changes in rigor bends was analyzed in detail. This method also enabled us to estimate the time course of the increase in the concentration of active dynein molecules *in situ*, which is important for an understanding of the presteady-state kinetics and chemo-mechanical coupling of dyneins (Johnson, 1985).

Materials and methods
Preparation of demembranated sperm flagella

Spermatozoa from the sea-urchin *Anthocidaris crassispina* were demembranated as described by Gibbons *et al.* (1982), with some modifications. Dry spermatozoa taken from the isolated gonad of the sea-urchin were suspended in 10 volumes of filtered natural sea water. The suspension was mixed with 10 volumes of extracting solution containing 0.04 % (w/v) Triton X-100, $0.2\,mol\,l^{-1}$ potassium acetate, $2\,mmol\,l^{-1}$ $MgCl_2$, $0.5\,mmol\,l^{-1}$ EGTA, $0.1\,mmol\,l^{-1}$ EDTA, $2\,mmol\,l^{-1}$ dithiothreitol (DTT) and $10\,mmol\,l^{-1}$ Tris–HCl (pH 8.0). The mixture was gently swirled for 30–60 s at room temperature (25 °C). After extraction, the suspension of demembranated sperm axonemes was introduced into a flow chamber constructed by placing a coverslip treated with dimethyldichlorosilane (Wako Pure Chemical, Osaka, Japan) onto a trough made from two pieces of Scotch tape (50 μm thick) glued in parallel 5 mm apart on a glass slide (76 mm×26 mm×0.9 mm). Reactivation solution containing $0.2\,mol\,l^{-1}$ potassium acetate, $2\,mmol\,l^{-1}$ $MgCl_2$, $0.5\,mmol\,l^{-1}$ EGTA, $0.1\,mmol\,l^{-1}$ EDTA, $4\,mmol\,l^{-1}$ DTT, $20\,mmol\,l^{-1}$ Hepes–KOH (pH 8.0) and 0.2 % (w/v) bovine serum albumin (BSA, A-0281, Sigma Chemical Co., St Louis, USA) without ATP was perfused through the chamber several times to wash out the extracting solution. The concentration of BSA in the reactivation solution was adjusted so that only the head region of the spermatozoon was loosely attached to the glass surface. The reactivation solution containing caged ATP (lot CL002, Dojindo, Kumamoto, Japan) and $0.4\,mg\,ml^{-1}$ apyrase (grade VII, Sigma Chemical Co., St Louis, USA) was then introduced into the chamber. Apyrase was used to remove contaminating ATP and/or ADP from caged ATP.

In addition to apyrase, $0.25\,i.u.\,\mu l^{-1}$ hexokinase (Grade I, Oriental Yeast Co., Osaka, Japan) and $0.1\,mmol\,l^{-1}$ glucose were added as an ATP-scavenger system to induce rigor-wave axonemes in a high-viscosity solution, since the abrupt removal of ATP was not possible by perfusion.

Experimental system

All the optical components of the microscope were aligned horizontally on an optical bench (Visolator, Meiritsu Seiki, Yokohama, Japan) (Fig. 1). A 100 W mercury arc lamp (UI-100, Ushio Electric Inc., Tokyo, Japan) was used as an ultraviolet source for the photolysis of caged ATP. The electromagnetic shutter (model no. 0, Copal, Tokyo, Japan) and filters (U-330 and UV-300, HOYA Optics, Tokyo, Japan) were placed between the arc lamp and a dichroic mirror (Asahi Spectra Co., Tokyo, Japan). The axonemes were irradiated with ultraviolet light under Koehler illumination conditions through the objective lens (D-Apo UV 100×, Olympus, Tokyo, Japan). The irradiated area was approximately 150 μm in diameter. The electromagnetic shutter was open for 10 ms. The percentage of photolysed caged ATP present in the solution after one ultraviolet pulse was estimated from the beat frequency of reactivated flagellar axonemes to be approximately 40 %. Flagellar axonemes were observed under dark-field illumination. The light source for the dark-field illumination was a 50 W tungsten–halogen lamp (from Optiphot-2, Nikon, Tokyo, Japan). To reduce ultraviolet light from the tungsten–halogen lamp, sharp cut-off filters (SC 50, Fuji Photo Film Corp., Tokyo, Japan) were placed in the light path between the lamp and an oil-immersion dark-field condenser (DC, Olympus, Tokyo, Japan). The movement of flagellar axonemes was recorded with a CCD camera (XC-73, Sony, Tokyo, Japan). An optical chopper driven by a stepping motor (PH 533 NA, Oriental Motor Corp., Tokyo, Japan) was put at the Lamsden disc of the eyepiece to record multiple images superimposed in each CCD image field. The rotation speed of the motor was controlled by horizontally synchronizing pulses

Fig. 1. A schematic diagram of the experimental system. All optical components are aligned on an optical bench. Vertically synchronizing pulses (V-sync pulse, 60 Hz) and horizontally synchronizing pulses (H-sync pulse, 15 750 Hz) from the CCD camera are introduced into a pulse controller to generate pulses which control the rotation of the optical chopper and the opening of the electromagnetic shutter, respectively. See text for further details.
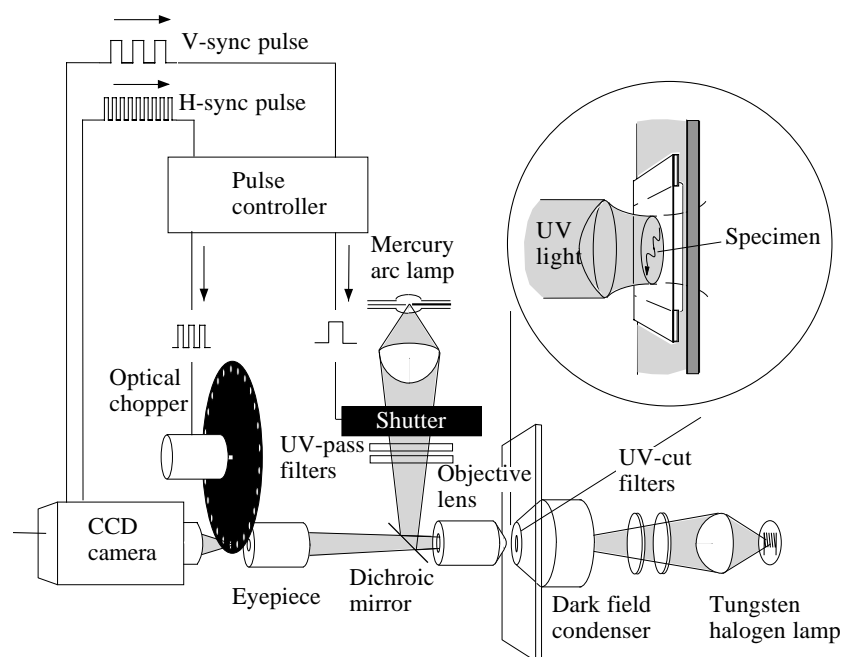
from the CCD camera so that the chopping rate was synchronized with the video rate. A chopping rate of up to 600 Hz was used (1–10 superimposed images per each field). The opening of the electromagnetic shutter for the photolysis of caged ATP was triggered by a vertically synchronizing pulse from the CCD camera. The opening time of the electromagnetic shutter was always adjusted to coincide with the appearance of the first image superimposed in the video field. Multiple superimposed images of flagella were recorded on Hi-8 video tapes using a video cassette recorder (EV-S1500 NTSC, Sony, Tokyo, Japan). During experiments, only spermatozoa whose beating plane was perpendicular to the optical axis were used for further analyses. All experiments were carried out at room temperature (25 °C).

Estimation of photo-released ATP concentration in the reactivation solution

The time course of ATP release from caged ATP was inferred from the rate of change of the characteristic transmission in 406 nm light (McCray *et al.* 1980), which was monitored using the same optical system and a photodiode (S 1557, Hamamatsu Photonics Co., Hamamatsu, Japan). The first 10 ms of transmission could not be recorded because of the excess ultraviolet used for photolysis and was, therefore, calculated by the temporal summation of the transmission change recorded with 1 ms ultraviolet pulses. Upon ultraviolet pulse application, transmission suddenly decreased and then increased exponentially with a rate constant of $35.6 \, \text{s}^{-1}$ at 25 °C. The ATP concentration curve after a 10 ms ultraviolet pulse was estimated as follows. The 10 ms duration of the ultraviolet pulse was divided into a number (n) of short durations, Δt. The fraction of total photoreleased ATP at time t is given by the summation of $[1 - e^{-35.6(t - i\Delta t)}]$ for an integer i from 0 to 10, where $i\Delta t \leqslant t$ and time 0 was taken as the time of starting the photolysis. The value

was calculated when $\Delta t = 1 \, \text{ms}$ and $n = 10$. The maximal concentration of photoreleased ATP was estimated from the beat frequency of reactivated spermatozoa. The change in ATP concentration in the reactivation solution was estimated, as shown in Fig. 2, from the measured time course of transmission change at 406 nm. The ATP concentration was expected to exceed a threshold level for the reactivation of motility within a few milliseconds and reached 90 % of the maximal level in 100 ms when $2 \, \text{mmol} \, \text{l}^{-1}$ caged ATP was used.

Data analysis

Recorded video images were fed into a personal computer (Power Macintosh 7600/120, Apple Computer Inc.) field by field for further analyses. In the digitized image, 10 pixels corresponded to 0.9 μm. The axes of the flagellar images and those of sperm heads were manually traced using the drawing software Canvas (ver. 2.1, Deneva Software). The traced images were then enlarged 2–3 times and transformed into a series of plots on an *x*–*y* plane using image-processing software (NIH Image, ver. 1.6/ppc). The *x*–*y* position of each divided segment of the axoneme (0.1–0.2 μm in length) was then determined from the base of the tail to its tip along the axoneme. The shear angle, the angle between the flagellar shaft and the axis of the sperm head, was then calculated from the *x*–*y* data for each segment. The accuracy of these procedures was checked using standard images of circles with curvatures
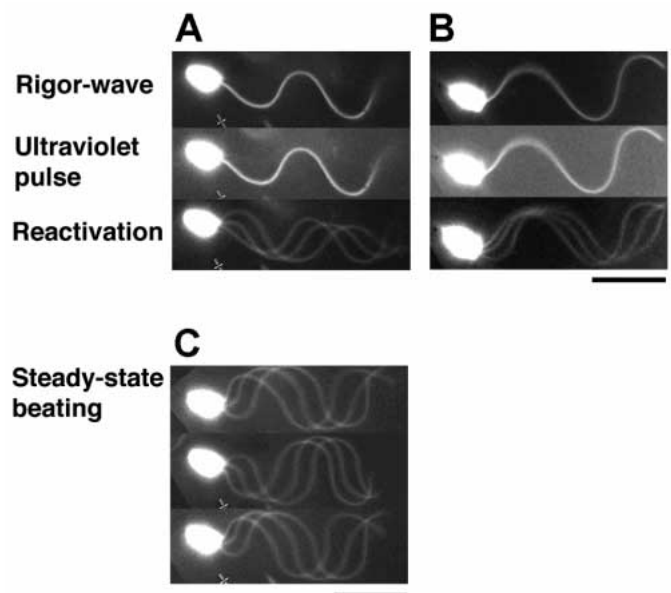
Fig. 3. Multiple superimposed dark-field images of demembranated sea-urchin sperm flagellar axonemes. (A,B) Flagella before and after the application of ATP by the rapid photolysis of $2 \, \text{mmol} \, \text{l}^{-1}$ caged ATP. (C) Flagellum showing continuous beating. Exposure frequency was $180 \, \text{s}^{-1}$, so that three images of flagella are superimposed onto each video field. Three successive fields are aligned from the top. For A and B, the first field shows rigor waves. The ultraviolet pulse was synchronized with the first image in the second field. Because of the time lag, reactivation was started from the first image in the third field. Scale bars, 10 μm.
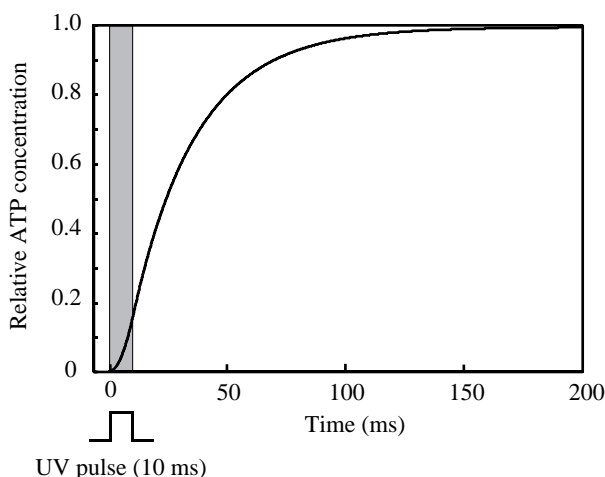

Fig. 2. Estimated photoreleased ATP concentration after the ultraviolet pulse. The rate constant was measured by the method of McCray *et al.* (1980), with some modifications. The transmission of light at 406 nm was measured after a 1 ms pulse of ultraviolet light for photolysis of $50 \, \text{mmol} \, \text{l}^{-1}$ caged ATP. See text for further details.

similar to those of flagellar bends. The error in determining shear angles was shown to be within ±0.08 rad. A series of shear angles was plotted against position along the axoneme. From these plots, designated as shear-curve plots, the peak-to-peak amplitudes between the maximal shear angles on both sides of a bend were measured as bend angles. The velocity of inter-doublet sliding of each axonemal segment along the flagellum was determined as $[A(t_1)-A(t_2)]/(t_1-t_2)$, where $A(t_1)$ and $A(t_2)$ are the shear angles of each segment at time t_1 and t_2, respectively. The time difference between t_1 and t_2 was 5.6 ms. The rigor bends were classified as principal or reverse bends on the basis of the asymmetric distribution of the shear angles of the bends after reactivation with reference to the head axis.

Results

Rapid reactivation of rigor-wave axonemes induced by the photolysis of caged ATP

Using caged ATP, a suprathreshold ATP concentration could be applied uniformly to demembranated sperm axonemes in rigor within a few milliseconds, as shown in

Fig. 2. Under the experimental conditions used, once reactivated by photolysis, axonemes continued steady-state beating for more than 1 min. After washing out ATP by perfusion, axonemes ceased beating, and the waveforms became frozen in a rigor state as described by Gibbons and Gibbons (1974a). These rigor waveforms remained unchanged for at least 30 min in the presence of caged ATP. Such reactivation and re-inactivation experiments could be repeated using a single demembranated spermatozoon. Fig. 3A,B shows dark-field images of flagellar axonemes before and after the application of ultraviolet pulses in reactivation solution containing $2\,\mathrm{mmol\,l^{-1}}$ caged ATP. Two typical cases where beating started from the principal bend (Fig. 3A) and from the reverse bend (Fig. 3B) at the basal region are shown. Irrespective of the phase in the rigor wave, all the rigor bends in the axonemes were observed to propagate in almost the same manner upon reactivation. The repropagation of bends occurred after a time lag of 11–17 ms, but a longer delay (approximately 22 ms) was always observed in the initiation of new bends at the basal region. No backward bend propagation was observed. Thus, after the rapid application of ATP, rigor-
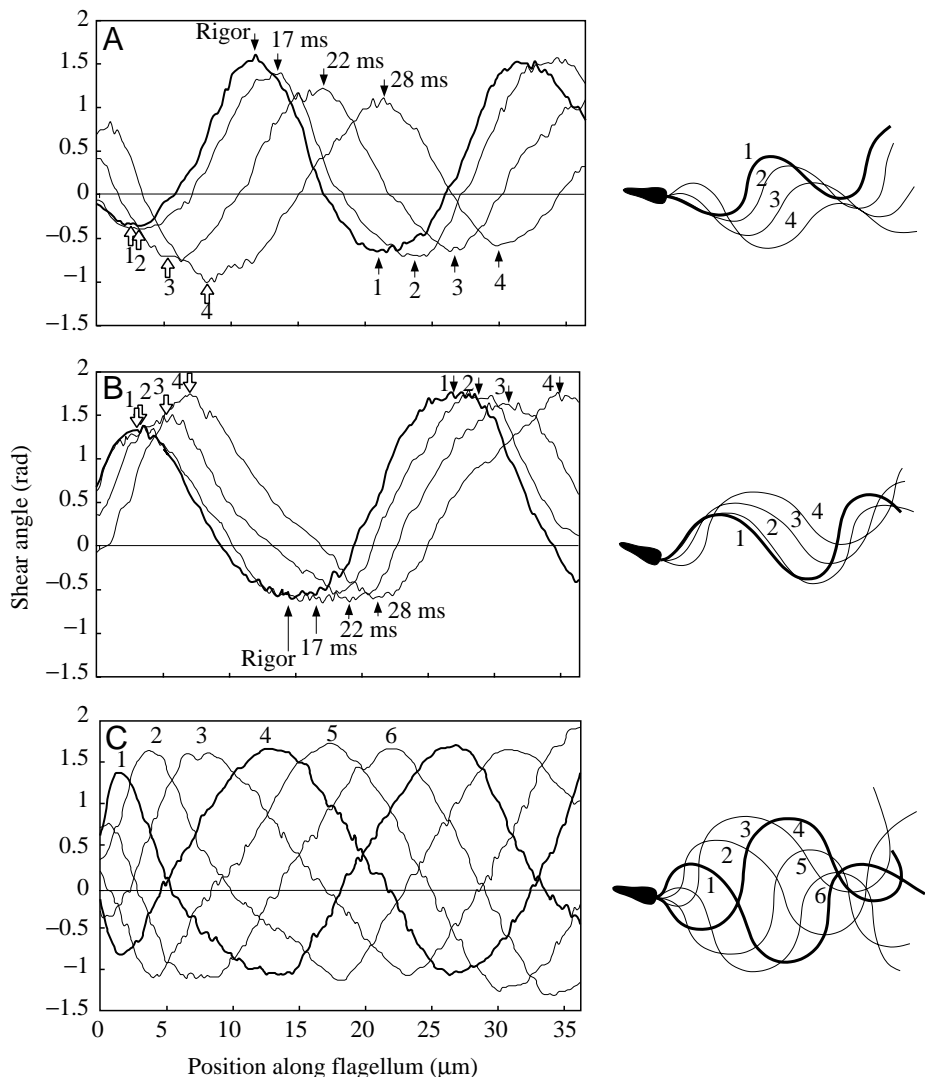

Fig. 4. Shear-curve transients after the rapid reactivation of sea-urchin sperm flagella. (A,B) Shear-curve plots obtained from flagellar waveforms before and after the application of ATP. (C) Plots obtained from flagellar waveforms of continuous beating. Since the exact angular direction at the base was obscured by excess light scatter from the head, the origin of the abscissa does not represent the first basal segment of the axoneme. In A and B, the curves obtained from the rigor waveform are shown as thick lines, which correspond to the thick lines shown on the spermatozoon on the right. Flagellar shear curves (left) and traces of waveforms (right) at 17, 22 and 28 ms after the initiation of ultraviolet pulses are shown as thin lines. In C, a series of flagellar shear curves is shown at intervals of 5.5 ms. The thick curves correspond to the thick lines shown on the traces on the right. See text for further details. Arrows mark maximal shear angles between developed (filled arrows) and undeveloped (open arrows) bends.
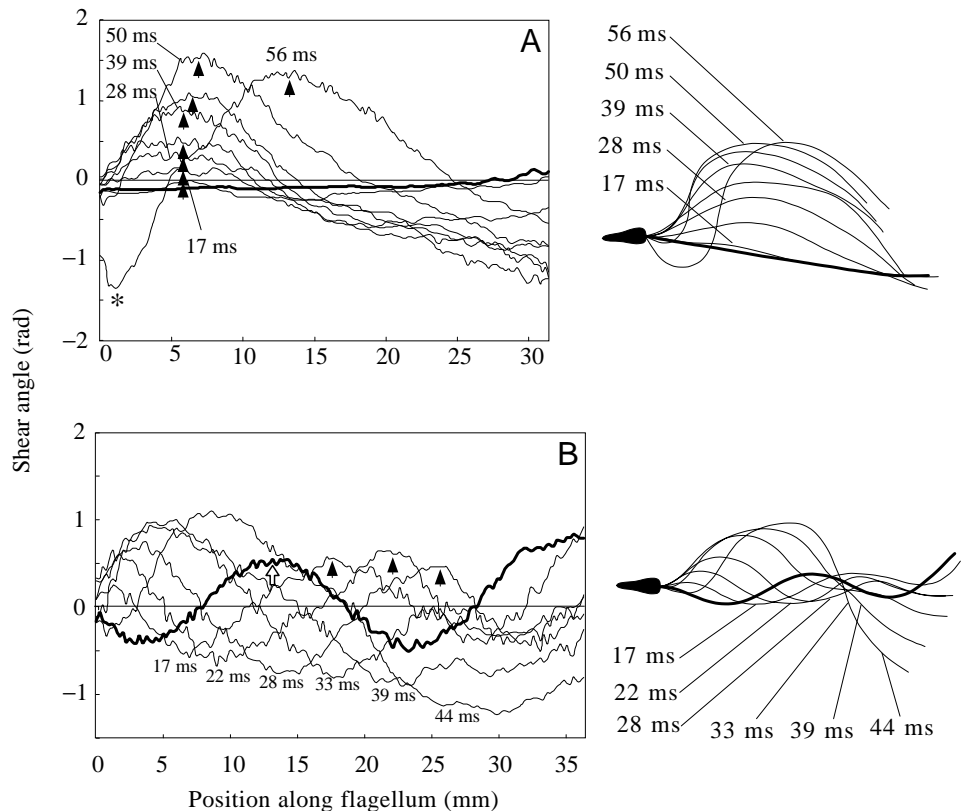
Fig. 5. Shear-curve transients obtained from a completely straightened flagellum (A) and a partially straightened flagellum (B) after rapid reactivation. The curves for rigor axonemes are expressed as thick lines, which correspond to the thick lines shown on the traces on the right. Flagellar shear curves (left) and traces of waveforms (right) at 17, 22, 28, 33, 39 and 44 ms (for A and B) and also at 50 and 56 ms (for A) after the start of ultraviolet pulses are presented as thin lines. The asterisk marks the maximum shear angle of the proximal reverse bend. See text for an explanation of the arrows.

wave axonemes began to beat as if they had been beating in steady state (Fig. 3C) without any pause.

Local angular change along the rigor-wave axonemes during the starting transients

For further detailed analyses, the transient of reactivation was examined using a shear-curve plot (Gibbons, 1982). The shear curve represents the degree of local sliding between the doublet microtubules when the bases of the axonemal microtubules are fixed if there is no significant compression or extensibility of the microtubules and if axonemal twist is negligible.

Shear-curve plots of four successive dark-field images taken during the starting transient (which correspond to the data in Fig. 3A,B, respectively) and the traces of superimposed waveforms are shown in Fig. 4A,B. After a time lag of 11–17 ms, the shear angles of almost all regions along the axoneme began to change. A longer time lag was observed at the proximal region, as shown by the shorter distance between the first two plots within 5 m of the basal region in Fig. 4A,B (lines 1 and 2). Peak positions of shear angle (indicated by filled arrows) were propagated towards the tip direction concomitantly with the initiation of local angular changes.

There are two types of bend along the axoneme: undeveloped bends and developed bends (Goldstein, 1976). In continuously beating sea-urchin sperm flagella, the amplitude of the shear angle (bend angle) gradually increases during the propagation of waves within approximately 10 μm of the base, and bends within this phase will be termed 'undeveloped bends'. After the bend angle has fully increased, the bend is propagated towards the tip with its bend angle almost unchanged, and bends in this phase will be termed 'developed bends'.

After rapid reactivation, the maximal shear angle between undeveloped bends in the rigor wave (indicated by open arrows in Fig. 4) began to increase. In contrast, those between the distal developed bends (indicated by filled arrows in Fig. 4) remained unchanged or even decreased during propagation. These characteristics of changes in the maximal shear angle at the starting transients were essentially the same as those for continuous beating (Fig. 4C).

Starting transients from straightened rigor axonemes

When the rigor-wave axonemes were immersed in a solution of ATP at a subthreshold concentration, the axonemes straightened. When the straightened rigor axonemes was reactivated in reactivation solution containing $2\,\mathrm{mmol\,l^{-1}}$ caged ATP, rather slower and quite different starting transients were observed compared with those of rigor-wave axonemes. Just after the ultraviolet pulse application, a large principal bend in the distal region and a small reverse bend in the proximal region were formed prior to bend propagation (Fig. 5A). The shear angle in the proximal region gradually increased (indicated by arrows) concomitantly with the increasing shear angle in the opposite direction at the distal region. The peak position of proximal shear angle was not propagated towards the tip until the maximal shear angle in the opposite direction was fully developed at the base (asterisk in Fig. 5A).
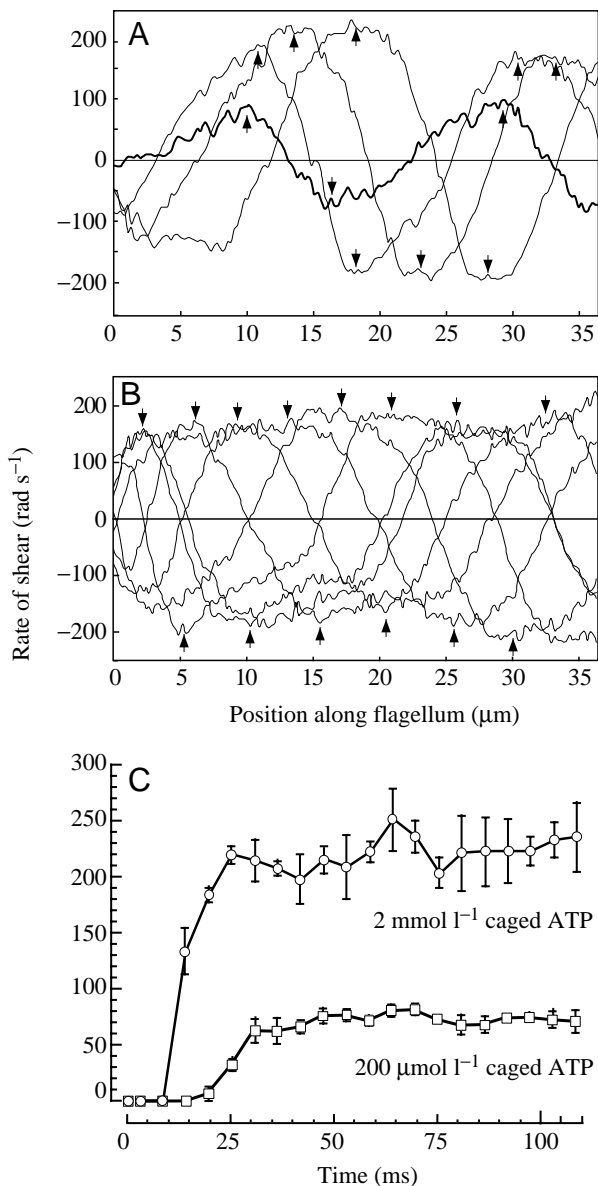
Fig. 6. The increase in the rate of angular change after rapid reactivation. (A) The rate of angular change (shear) plotted against the position along the axoneme. The first recording after rapid ATP application is shown as a thick line and the following three recordings are shown as thin lines. Filled arrows indicate the positions of the maximal rates on both the reverse and principal sides of the bend. (B) The rate of angular change (shear) along the axoneme during steady-state beating. The maximum shear rate in both the upward (principal side) and the downward (reverse side) direction were almost constant along the axoneme in any phase of the beating cycle, except in the regions within approximately 5 μm of the end of the base and tip. (C) The maximal rate of angular change (shear) measured in a 5–35 μm region of the axoneme plotted against time after the start of the ultraviolet pulse (duration 10 ms). Data from 2 mmol l^{-1} caged ATP (○; $N=3$) and 200 μmol l^{-1} caged ATP (□; $N=3$) are shown. Values are means and standard deviations.

We also examined starting transients of reactivation from partially straightened rigor-wave axonemes, which contained rigor bends with a small bend angle of less than 1 rad (compared

with a bend angle of up to 2.5 rad during continuous beating in Fig. 4C). As shown in the traces in Fig. 5B, rapid repropagation of bends was started while the elongated waveforms were maintained. Although the bend angles and maximal shear angles at the pre-existing distal bends were small (indicated by an open arrow in Fig. 5B), bends were propagated towards the tip with no increase in the bend angle and maximal shear angle (indicated by filled arrows in Fig. 5B).

Time course of the increase in the rate of tubule sliding after the photolysis of caged ATP

The time course of the increase in the rate of tubule sliding after the photolysis of 2 mmol l^{-1} caged ATP was estimated from the rate of change in shear angle. As shown in Fig. 6A, the maximal rate of shear gradually increased as the wave was propagated towards the tip (filled arrows). In steady-state beating, in comparison, the maximal rate of shear was almost constant at any site along the axoneme (Fig. 6B, indicated by filled arrows) except at the base, where the bend was being developed, and at the tip, where the maximal shear angle was somewhat larger than in other regions. From these data, time courses of the increase in the maximal shear rate (except for the region within 5 μm of the base and tip of the axoneme) were plotted (Fig. 6C). The shear rate began to increase after a time lag of 11–17 ms after the ultraviolet pulse and reached a plateau value (approximately 220 rad s^{-1}) within 28 ms. The plateau value corresponds to a maximal velocity of tubule sliding of approximately 11 μm s^{-1}, providing that the sliding distance is given by φd, where φ is the local shear angle and d (approximately 50 nm) is the spacing between the pair of tubules projected onto the beat plane. Beat frequency was approximately 30 Hz when the shear rate reached the plateau value. Given the time course of ATP release after photolysis (Fig. 2), ATP release from caged ATP was unlikely to have a major rate-limiting effect on the time lag we observed.

When reactivation solution containing 200 μmol l^{-1} caged ATP was used, rather slower starting transients were observed. The rigor waves were repropagated 17–22 ms after the ultraviolet pulse. The maximal rate of angular change within an axoneme increased to reach a plateau level of approximately 70 rad s^{-1} (estimated sliding velocity 3.5 μm s^{-1}) within 33 ms.

Effects of external viscous load on bend initiation and bend propagation after rapid reactivation

External viscous load is known to affect the waveforms of beating axonemes by altering the maximal shear angle and curvature (Brokaw, 1966, 1996). In the present paper, we examined the effects of external viscous load on the rapid reactivation of rigor axonemes by adding 2% methylcellulose (M-0387, Sigma Chemical Co., 1500 mPa s at 25 °C) to the reactivation solution containing 2 mmol l^{-1} caged ATP. In Fig. 7A,B, typical starting transients of rapidly reactivated axonemes in high-viscosity solution are shown. As expected, the rigor waves formed under high-viscosity conditions were similar to those formed in the normal reactivation solution at lower viscosity since the
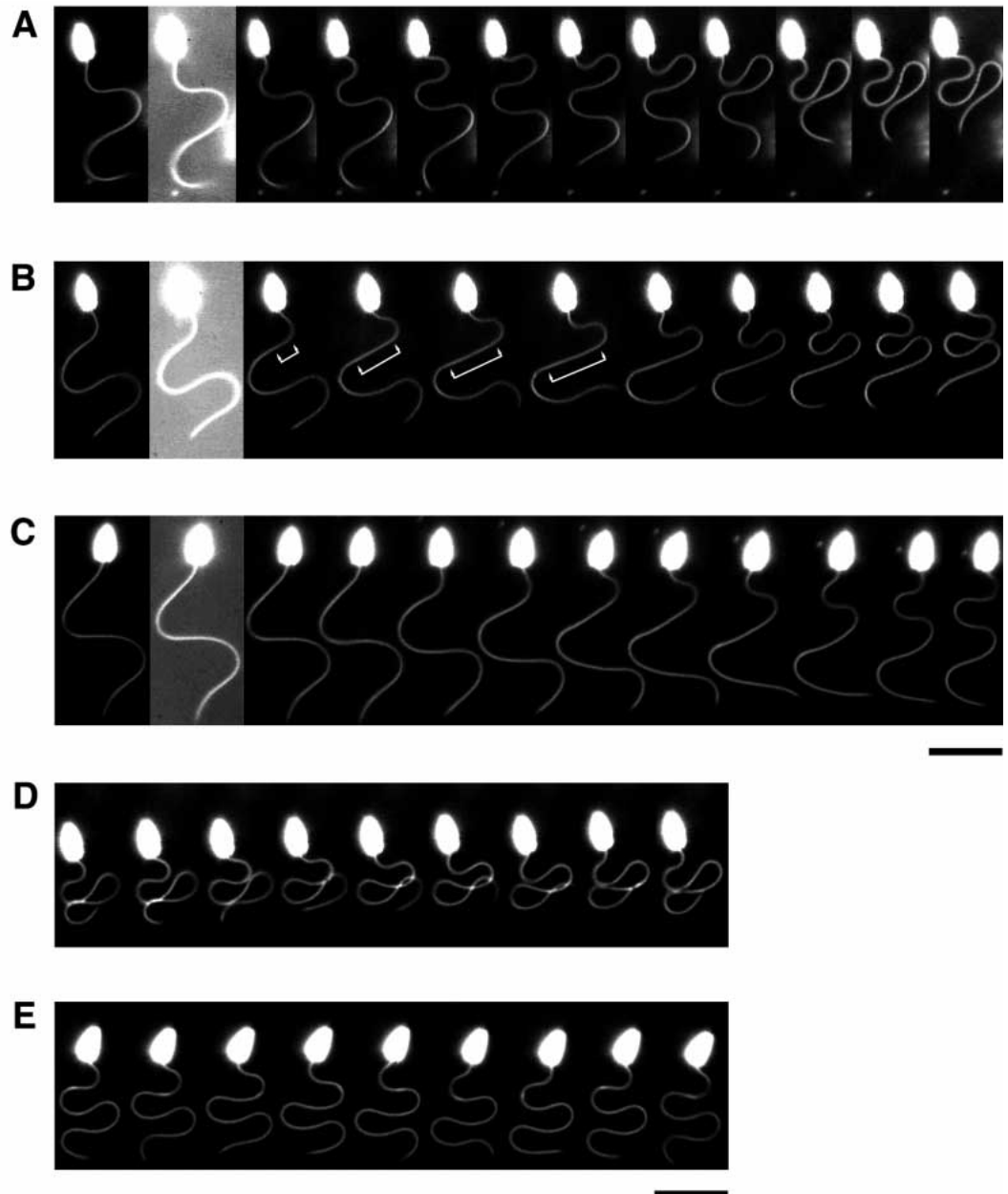
Fig. 7. Starting transients after reactivation by photolysis of caged ATP under high-viscosity condition (1500 mPa s at 25 °C). Examples of the starting transient when the sperm heads were firmly attached to the glass surface (A,B) and of the starting transient when the spermatozoon was swimming freely (C) are shown. (D,E) Flagella showing continuous beating under high-viscosity condition (D, head attached; E, swimming freely). Video frames at intervals of 33 ms in series were aligned from left to right. In A, B and C, the first frame shows the rigor waves. A 10 ms ultraviolet pulse was introduced at the second frame, and subsequent reactivation is shown in the following frames. In B, straightened interbend regions are indicated by open arrows. Scale bars, 10 μm.

waveforms in rigor axonemes are determined under conditions of extremely low ATP concentration, where the external viscous load has been shown to have little effect on waveform (Brokaw, 1975). As under conditions of normal viscosity, reactivation in high-viscosity fluid was observed after a time lag of 11–17 ms from the beginning of the ultraviolet pulse, and all rigor bends in the axoneme were propagated only towards the tip. This result suggests that the time lag before reactivation is not due to the external viscous load, but reflects the kinetics of the rate of activation. When straightened rigor axonemes were rapidly reactivated under the same viscosity condition, axonemes were often observed to break at the base before the bends were formed (data not shown).

During the starting transient of reactivation under the high viscous load, quite different responses were observed between the bend initiation and bend propagation processes. As shown in Fig. 7A,B, at the starting phase of reactivation, the undeveloped rigor bends began to change their form into those typical of steady-state beating under high-viscosity condition (Fig. 7D). In contrast to the undeveloped bends, the fully developed rigor bends were repropagated with their pre-existing forms almost unchanged until they disappeared at the tip of the axoneme.

Shear-curve plots during the starting transients also showed the different responses of rigor bends in proximal and distal regions (Fig. 8A,B). The maximal shear angle on the proximal side of undeveloped rigor bends, or in newly formed bends, gradually increased to approximately 2–2.5 rad (indicated by open arrows in Fig. 8A,B), which is as high as the maximal shear angle observed in steady-state beating under high-viscosity condition (Fig. 8C). In contrast, the maximal shear angles on both sides of
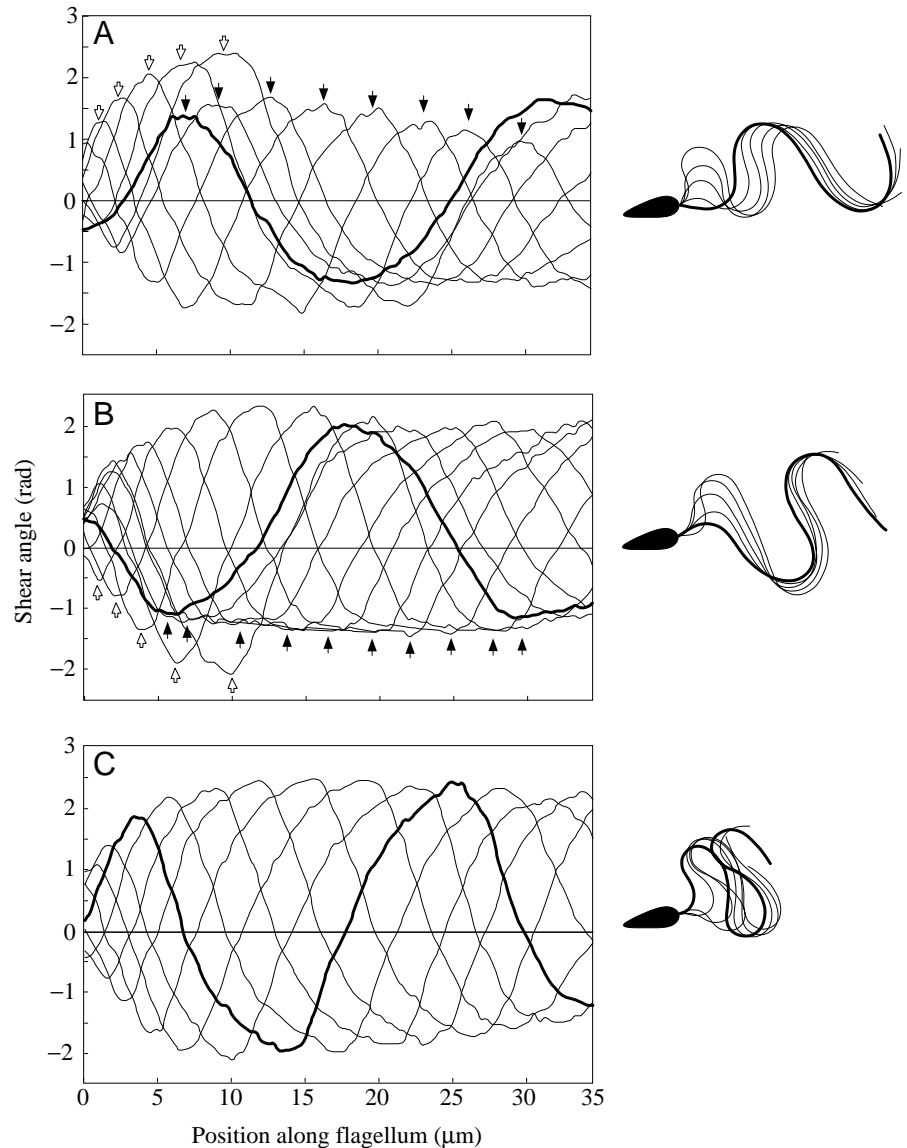
Fig. 8. Shear-curve transients obtained from reactivated rigor-wave sea-urchin sperm flagella under high-viscosity conditions (A,B). (C) Curves obtained from a flagellum showing continuous beating. In A and B, the shear curves of the rigor wave are shown as thick lines, corresponding to the thick traces on the right. A series of shear curves (left) and traces of the waveforms (right) after the reactivation are shown using thin lines. In C, the shear curve with a thick line corresponds to the trace with a thick line on the right. Curves and traces at intervals of 33 ms are shown with thin lines. See text for further details.

the fully developed rigor bend remained almost constant until the end of propagation (indicated by filled arrows in Fig. 8A,B). Straight interbend regions became wider (indicated by arrows in Fig. 7B) if the rapid reactivation was started from a rigor wave with an undeveloped principal bend at the basal region. This interbend region is represented as a flattened plateau of shear curves in Fig. 8B (filled arrows) and was not observed when the rapid reactivation was started from a rigor axoneme with an undeveloped reverse bend at the basal region (Figs 7A, 8A).

Although these results were obtained from demembranated sperm flagella whose heads were firmly attached to a glass slide, the starting transients of freely swimming flagella were observed to be essentially similar (Fig. 7C, starting transient; Fig. 7E, steady-state beating).

Discussion

Caged ATP was used to examine how bends were initiated and propagated in sea-urchin sperm flagella in a state of rigor. The advantage of using caged ATP is that the whole length of the flagellar axoneme can be simultaneously influenced by a rapid and homogeneous increase in ATP concentration, and dynein ATPase activity is expected to be initiated in a synchronized manner, even in a high-viscosity solution. This enabled us to examine the relationship between dynein ATPase cycling and the initiation of tubule sliding. The waveforms after photolysis of caged ATP were essentially the same as those observed when the axonemes were slowly reactivated by perfusion with an ATP-containing solution (Gibbons and Gibbons, 1974a; Goldstein, 1979).

Upon rapid reactivation by photolysis of caged ATP, the maximal rate of angular change, which corresponds to the maximal velocity of tubule sliding in the axoneme, reached a plateau value within 28 ms of the beginning of the ultraviolet pulse when the estimated maximal ATP concentration was $0.8\,\mathrm{mmol\,l^{-1}}$ (Fig. 6). This rate of onset of the power-stroke of
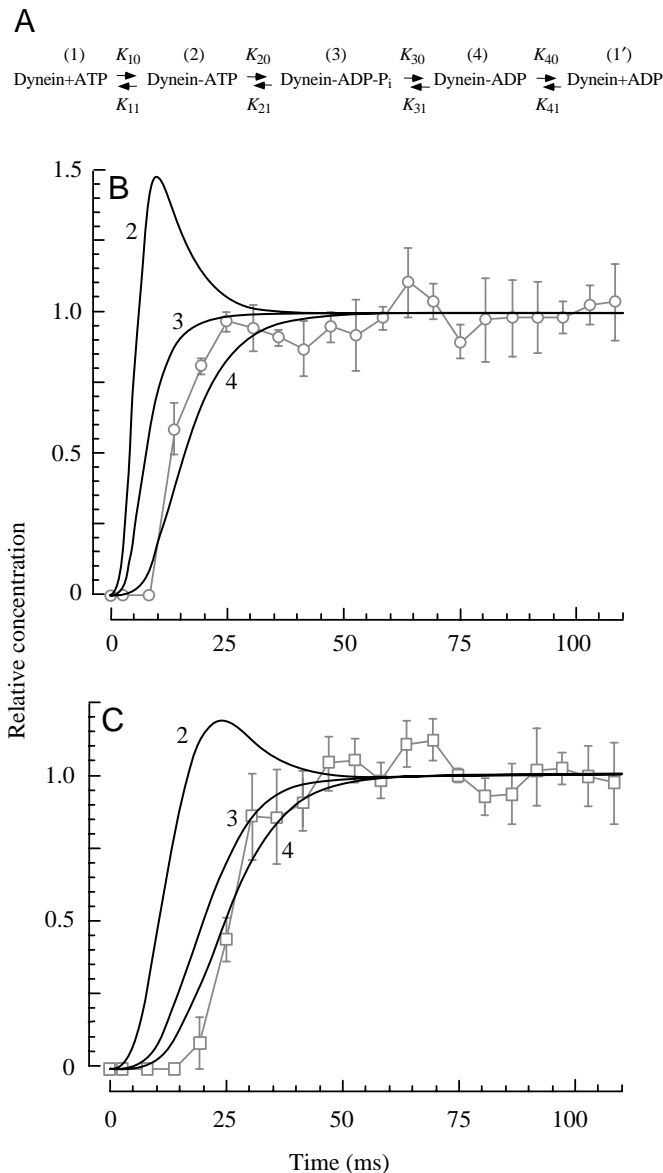
Fig. 9. Estimation of the increasing concentration of active dynein in the axoneme. (A) A kinetic scheme of the elementary steps of dynein ATPase (Johnson, 1985). (B,C) Simulation of the increase in [dynein-ATP] (step 2), [dynein-ADP-P_i] (step 3) and [dynein-ADP] (step 4) after the photolysis of $2\,\mathrm{mmol\,l^{-1}}$ (B) and $200\,\mathrm{\mu mol\,l^{-1}}$ (C) caged ATP. Rate constants, $K_{10}=4\,\mathrm{s^{-1}\,l\,\mu mol^{-1}}$, $K_{11}=0.15\,\mathrm{s^{-1}}$, $K_{20}=50\,\mathrm{s^{-1}}$, $K_{21}=3\,\mathrm{s^{-1}}$, $K_{30}=70\,\mathrm{s^{-1}}$, $K_{31}=8000\,\mathrm{s^{-1}}$ and $K_{41}=0.015\,\mathrm{s^{-1}\,l\,\mu mol^{-1}}$ were used. A rate constant of $200\,\mathrm{s^{-1}}$ was used for K_{40}, given the increase in the rate of ADP release from dynein in the presence of microtubules. The time course of the increase in the concentration of photoreleased ATP (Fig. 2) was used for the calculation. The time courses of the increase in the measured sliding velocity (taken from Fig. 6) are expressed as half-tone plots. All the curves are normalized by putting the value at $t=100\,\mathrm{ms}$ to 1.0.

On the basis of the reported kinetics of dynein ATPase (Johnson, 1985), the increase in sliding velocity after the rapid application of ATP is assumed to reflect the presteady-state dynein activity together with the start of a new cycle of ATP hydrolysis. Under load-balanced condition, i.e. when the force exerted by dynein is always balanced by a viscous or elastic load, the observed velocity of tubule sliding should be proportional to the sliding force. If this is the case in our experiments, and the force exerted by the axoneme is assumed to be proportional to the population of active dynein arms, we can estimate a kinetic rate related to the power stroke from the time course of the increasing velocity of tubule sliding. By employing the kinetic rates reported previously from purified *Tetrahymena* 22S dynein ATPase (Johnson, 1983; Porter and Johnson, 1983; Holzbaur and Johnson, 1989*a*), we calculated how the concentrations of dynein-ATP, dynein-ADP-P_i and dynein-ADP changed. The calculation was carried out taking into account the time course of the increase in ATP concentration (Fig. 2). As shown in Fig. 9B, the estimated time course of the increase in concentration of dynein-ADP-P_i and dynein-ADP fitted well with the data obtained if the rate constant of ADP release from dynein is increased to approximately $200\,\mathrm{s^{-1}}$, the rate previously reported from biochemical analyses in the presence of microtubules (Omoto and Johnson, 1986; Holzbaur and Johnson, 1989*b*; Shimizu *et al.* 1989). The time course obtained at a lower concentration of ATP (Fig. 9C, squares) also fitted well with the estimated time courses of [dynein-ADP-P_i] and [dynein-ADP] when the rate of ADP release from dynein was also accelerated. This is the first estimation of the kinetics of force generation by dynein *in situ*.

There are, however, several possibilities that would lead to an over- or underestimate of the rate of increase in the number of active dynein arms. First, the rate would be overestimated if tubule sliding occurred under conditions of low loading, where sliding velocity could reach a plateau earlier with a lower number of active dynein arms since velocity is assumed to reflect the intrinsic stroke rate of dynein itself and not to correspond to the magnitude of exerted forces. In addition, caged ATP has been reported to be a competitive inhibitor of ATP-driven sliding of actomyosin (Thirlwell *et al.* 1995) and kinesin (Higuchi *et al.* 1997). In our preliminary experiments, caged ATP was shown to lower the beat frequency of reactivated flagella, with an estimated inhibition constant of $1.0–1.4\,\mathrm{mmol\,l^{-1}}$ (data not shown), and this inhibitory effect of caged ATP could lead to an underestimation of the rate. From the kinetic analysis of the dynein ATPase pathway, a change in conformation is thought to occur during the dynein-ADP state (Holzbaur and Johnson, 1989*a*). However, dynein-ADP-P_i is believed to be a state with a conformation different from that of nucleotide-free dynein (Inaba and Mohri, 1989). Further detailed physiological investigations are required to determine the exact correlation between the intermediate kinetics and force generation by dynein.

After rapid application of ATP, flagella started to propagate the remaining rigor bends towards the tip, as in steady-state

dynein is much slower than the rate expected from the high-frequency (>300 Hz) nanometre-scale oscillation of flagellar axonemes observed by Kamimura and Kamiya (1989, 1992), the mechanism of which has yet to be clarified.

beating. This result suggested that the profiles of the active and inactive sites of microtubule sliding in the axoneme were conserved, even during complete depletion of ATP, and could be reinstated during the initial turnover cycle of ATP. In contrast to the rapid reinstatement in rigor-wave axonemes, slower transients of reactivation were observed in completely straightened rigor axonemes (Fig. 5A). After the ultraviolet pulse, a large principal bend at the distal region and a small reverse bend at the proximal region were formed gradually at first. These bends were not propagated until the reverse bend was fully developed at the basal region. During the formation of these bends, tubule slidings of opposite direction were thought to occur concomitantly at the proximal and the distal regions. A similar starting transient was reported for straightened live sperm flagella activated by a sudden increase in extracellular pH (Goldstein, 1979).

From our data, the velocity of sliding during the initial bend formation was much slower (approximately $50 \, \mathrm{rad \, s^{-1}}$) than that after bend propagation had started (approximately $220 \, \mathrm{rad \, s^{-1}}$). This result indicates that the existence of remaining bends in the rigor axonemes is important for the fluent reactivation of tubule sliding after the rapid application of ATP. A rapid increase in sliding velocity was observed when only a small bend (<1 rad) existed in the rigor axonemes (Fig. 5B).

The observation of wave propagation of such small bends also showed how pre-existing bends are conserved during the starting transients of reactivation. Although the bend angles and maximal shear angles in these cases were much smaller than those in steady-state beating, they remained almost constant during propagation. Thus, the bend angles and maximal shear angles of distal bends were predominantly affected by those of pre-existing rigor bends. This was clearly observed when the rapid reactivation was triggered in high-viscosity solution, where the new bends forming after reactivation were completely different from the pre-existing rigor bends. As shown in Fig. 8, in the distal region of the axoneme, additional tubule shearing did not occur beyond the maximal shear amplitude of pre-existing rigor waves even under conditions where the shear amplitude could be increased by viscous load. These data also suggested different responses to external viscous load between bend initiation and bend propagation mechanisms. The propagation of a constant bend angle has also been observed in live starfish sperm flagellum when the development of bending in the proximal region was artificially restricted by glass needles (Okuno and Hiramoto, 1976).

It is possible that the viscous bending moment is acting predominantly on the proximal region of the axoneme, and this causes the enhanced responses of the proximal region to the viscous load. Although we calculated the bending moment of reactivating axonemes on the basis of resistive force theory (Gray and Hancock, 1955; Baba and Hiramoto, 1970), we found little correlation between the magnitude of the bending moment and the waveform. Rather than using calculations based on resistive force theory, detailed calculations using

stokeslet flow-fields (Lighthill, 1996) or boundary element methods (Ramia *et al.* 1993; Goto *et al.* 1997) may be required to obtain further insight into the hydrodynamic aspects of flagellar bending.

We used the photolysis of caged ATP to examine the initial transients of rapid reactivation and indirectly monitored the increase in sliding velocity from angular changes in the axonemes. This enabled us to detect the minute shear of tubules below the level of optical resolution (<200 nm) during the starting transients. This technique could be used in combination with nanometre-scale detecting methods (Kamimura, 1987) to examine other simple system of motility and to gain greater insight into the chemo-mechanical coupling of dynein.

References

BABA, S. A. AND HIRAMOTO, Y. (1970). A quantitative analysis of ciliary movement by means of high-speed microcinematography. *J. exp. Biol.* **52**, 675–690.

BROKAW, C. J. (1966). Effects of increased viscosity on the movements of some invertebrate spermatozoa. *J. exp. Biol.* **45**, 113–139.

BROKAW, C. J. (1975). Effects of viscosity and ATP concentration on the movement of reactivated sea-urchin sperm flagella. *J. exp. Biol.* **62**, 701–719.

BROKAW, C. J. (1989). Direct measurements of sliding between outer doublet microtubules in swimming sperm flagella. *Science* **243**, 1593–1596.

BROKAW, C. J. (1996). Microtubule sliding, bend initiation and bend propagation parameters of *Ciona* sperm flagella altered by viscous load. *Cell Motil. Cytoskel.* **33**, 6–21.

BROKAW, C. J. AND BENEDICT, B. (1968). Mechanochemical coupling in flagella. I. Movement-dependent dephosphorylation of ATP in glycerinated spermatozoa. *Archs Biochem. Biophys.* **125**, 770–778.

GIBBONS, B. H. AND GIBBONS, I. R. (1972). Flagellar movement and adenosine triphosphatase activity in sea urchin sperm extracted with Triton X-100. *J. Cell Biol.* **54**, 78–97.

GIBBONS, B. H. AND GIBBONS, I. R. (1974a). Properties of flagellar 'rigor waves' formed by abrupt removal of adenosine triphosphate from actively swimming sea urchin sperm. *J. Cell Biol.* **63**, 970–985.

GIBBONS, B. H. AND GIBBONS, I. R. (1974b). The fine structure of rigor wave axonemes from sea-urchin sperm flagella. *J. Cell Biol.* **63**, 110A.

GIBBONS, I. R. (1982). Sliding and bending in sea urchin sperm flagella. In *Symposium of the Society for Experimental Biology,* vol. 35, *Prokaryotic and Eukaryotic Flagella* (ed. W. B. Amos and J. G. Duckette), pp. 225–287. Cambridge: Cambridge University Press.

GIBBONS, I. R., EVANS, J. A. AND GIBBONS, B. H. (1982). Acetate anions stabilize the latency of dynein 1 ATPase and increase the

velocity of tubule sliding in reactivated sperm flagella. *Cell Motil. Suppl.* **1**, 181–184.

GIBBONS, I. R. AND ROWE, H. J. (1965). Dynein: A protein with adenosine triphosphatase activity from cilia. *Science* **149**, 424–426.

GOLDMAN, Y. E., HIBBERD, M. G., MCCRAY, J. A. AND TRENTHAM, D. R. (1982). Relaxation of muscle fibres by photolysis of caged ATP. *Nature* **300**, 701–705.

GOLDSTEIN, S. F. (1976). Form of developing bends in reactivated sperm flagella. *J. exp. Biol.* **64**, 173–184.

GOLDSTEIN, S. F. (1979). Starting transient in sea urchin sperm flagella. *J. Cell Biol.* **80**, 61–68.

GOTO, T., TAGA, Y. AND TAKANO, Y. (1997). Study on relative force theory for flagella with boundary element method. *Trans. Jap. Soc. Mech. Eng.* **63**, no. 605B, 188–193.

GRAY, J. AND HANCOCK, G. J. (1955). The propulsion of sea-urchin spermatozoa. *J. exp. Biol.* **32**, 802–814.

HIGUCHI, H., MUTO, E., INOUE, Y. AND YANAGIDA, T. (1997). Kinetics of force generation by single kinesin molecules activated by laser photolysis of caged ATP. *Proc. natn. Acad. Sci. U.S.A.* **94**, 4395–4400.

HOLZBAUR, E. L. AND JOHNSON, K. A. (1989*a*). ADP release is rate limiting in steady-state turnover by the dynein adenosinetriphosphatase. *Biochemistry* **28**, 5577–5585.

HOLZBAUR, E. L. AND JOHNSON, K. A. (1989*b*). Microtubules accelerate ADP release by dynein. *Biochemistry* **28**, 7010–7016.

INABA, K. AND MOHRI, H. (1989). Dynamic conformational changes of 21S dynein ATPase coupled with ATP hydrolysis revealed by proteolytic digestion. *J. biol. Chem.* **264**, 8384–8388.

JOHNSON, K. A. (1983). The pathway of ATP hydrolysis by dynein: kinetics of a presteady state phosphate burst. *J. biol. Chem.* **258**, 13825–13832.

JOHNSON, K. A. (1985). The pathway of the microtubule-dynein ATPase and the structure of dynein: a comparison with actomyosin. *A. Rev. biophys. biophys. Chem.* **14**, 161–188.

KAMIMURA, S. (1987). Direct measurement of nanometric displacement under an optical microscope. *Appl. Optics* **26**, 3425–3427.

KAMIMURA, S. AND KAMIYA, R. (1989). High-frequency nanometre-scale vibration in 'quiescent' flagellar axonemes. *Nature* **340**, 476–478.

KAMIMURA, S. AND KAMIYA, R. (1992). High-frequency vibration in flagellar axonemes with amplitudes reflecting the size of tubulin. *J. Cell Biol.* **116**, 1443–1454.

KAPLAN, J. H., FORBUSH III, B. AND HOFFMAN, J. H. (1978). Rapid photolytic release of adenosine 5′-triphosphate from a protected analogue: Utilization by the Na:K pump of human red blood cell ghosts. *Biochemistry* **17**, 1929–1935.

LIGHTHILL, J. (1996). Reinterpreting the basic theorem of flagellar hydrodynamics. *J. Eng. Math.* **30**, 25–34.

MCCRAY, J. A., HERBETTE, L., KIHARA, T. AND TRENTHAM, D. R. (1980). A new approach to time-resolved studies of ATP-requiring biological systems: laser flash photolysis of caged ATP. *Proc. natn. Acad. Sci. U.S.A.* **77**, 7237–7241.

OKUNO, M. AND HIRAMOTO, Y. (1976). Mechanical stimulation of starfish sperm flagella. *J. exp. Biol.* **65**, 401–413.

OMOTO, C. K. AND JOHNSON, K. A. (1986). Activation of the dynein adenosine triphosphatase by microtubules. *Biochemistry* **25**, 419–427.

PORTER, M. E. AND JOHNSON, K. A. (1983). Transient state kinetic analysis of the ATP-induced dissociation of the dynein–microtubule complex. *J. biol. Chem.* **258**, 6582–6587.

RAMIA, M., TULLOCK, D. L. AND PHAN-THIEN, N. (1993). The role of hydrodynamic interaction in the locomotion of microorganisms. *Biophys. J.* **65**, 755–778.

SALE, W. S. AND SATIR, P. (1977). The direction of active sliding of microtubules in *Tetrahymena* cilia. *Proc. natn. Acad. Sci. U.S.A.* **74**, 2045–2049.

SATIR, P. (1968). Studies on cilia. III. Further studies on the cilium tip and a 'sliding filament' model of ciliary motility. *J. Cell Biol.* **39**, 77–94.

SHIMIZU, T., MARCHESE-ROGANA, S. P. AND JOHNSON, K. A. (1989). Activation of the dynein adenosine triphosphatase by cross-linking to microtubules. *Biochemistry* **28**, 7016–7021.

SHINGYOJI, C., MURAKAMI, A. AND TAKAHASHI, K. (1977). Local reactivation of Triton-extracted flagella by iontophoretic application of ATP. *Nature* **265**, 269–270.

SUMMERS, K. E. AND GIBBONS, I. R. (1971). Adenosine triphosphate-induced sliding of tubules in trypsin-treated flagella of sea-urchin sperm. *Proc. natn. Acad. Sci. U.S.A.* **68**, 3092–3096.

THIRLWELL, H., SLEEP, J. A. AND FERENCZI, M. A. (1995). Inhibition of unloaded shortening velocity in permeabilized muscle fibres by caged ATP compounds. *J. Muscle Res. Cell Motil.* **16**, 131–137.

WOOLLEY, D. M. AND BOZKURT, H. H. (1995). The distal sperm flagellum: its potential for motility after separation from the basal structures. *J. exp. Biol.* **198**, 1469–1481.